MJFAS
Malaysian Journal of Fundamental and Applied Sciences



RESEARCH ARTICLE

# Activated Biopolymers from Trigona Honeycomb Waste: Structural Characterization and Potential for Sustainable Agricultural Materials

**Irwan Ramli[a,*], Hilda Rahmawati[a], Siti Nurmiati[b], Fitrah Al-Anshori[c], Yanuar Sigit Pramana[d], Sukarti[b], , Rapiah[a], Silfa Azzahra[a]**

[a]Department of Physics, Faculty of Science, Universitas Cokroaminoto Palopo, 91922, South Celebes, Indonesia, [b]Department of Chemistry, Faculty of Science, Universitas Cokroaminoto Palopo, 91922, South Celebes, Indonesia, [c]Department of Biology Education, Faculty of Teacher Training and Education, Universitas Cokroaminoto Palopo, 91922, South Celebes, Indonesia, [d]Research Center for Process Technology, National Research and Innovation Agency (BRIN), South Tangerang 15314, Banten, Indonesia. Indonesia

Abstract This study investigates the isolation, activation, and physicochemical characterization of natural biopolymers derived from Trigona honeycomb waste, an underutilized biomass resource with potential value-added applications. The biopolymer was extracted through sequential processes including acid hydrolysis, chlorination, alkaline treatment, and bleaching, followed by chemical activation using a mixed solution of sulfuric acid ($H_2SO_4$) and acetic acid ($CH_3COOH$). Structural and compositional analyses were conducted using XRF, XRD, FTIR, and SEM.

XRF results revealed that calcium (Ca) is the dominant component, increasing from 46.6% before activation to 54.8% after activation, indicating enhanced mineral exposure due to structural modification. XRD patterns showed characteristic diffraction peaks at $2\theta \approx 11.65°$, 14.81°, 15.99°, 20.81°, and 23.23°, confirming a semi-crystalline Type I biopolymer structure. FTIR spectra identified functional groups typical of natural biopolymers, including hydroxyl (-OH), aliphatic C–H, and C–O–C bonds, suggesting the presence of polysaccharide-based structures. SEM images demonstrated significant morphological changes after activation, with increased surface roughness and the formation of microcavities, which are associated with higher surface area.

These findings indicate that chemical activation significantly alters both the structural and surface properties of the biopolymer, enhancing its potential as a functional biomass precursor. The improved physicochemical characteristics suggest its prospective application in controlled nutrient delivery systems, particularly for sustainable agricultural materials.

**Keywords**: Trigona honeycomb waste, Natural biopolymer, Chemical activation, Physicochemical characterization, Biomass valorization.

***For correspondence:**
irwan@uncp.ac.id

**Received:** 01 May. 2026
**Accepted:** 10 Aug 2026



## Introduction

Natural biopolymers have attracted considerable attention due to their biodegradability, low toxicity, and renewability. Natural biopolymers have attracted considerable attention owing to their biodegradability, low toxicity, and renewability, making them promising materials for a wide range of sustainable applications. [1,2]. In recent years, the shift toward biomass valorization has encouraged the exploration of unconventional and underutilized resources as alternative raw materials [3,4]. One such resource is waste derived from *Trigona* honeycombs, which remains largely overlooked despite its complex biochemical composition [5,6].

*Trigona* bees, commonly known as stingless bees, are widely distributed across tropical regions and play a crucial ecological role as pollinators [7]. In addition to producing honey, pollen, and propolis,

these bees construct honeycombs composed of a heterogeneous matrix of plant resins, waxes, and enzymatically modified organic substances. This unique structural composition suggests that *Trigona* honeycomb waste may serve as a promising precursor for natural biopolymer extraction. However, compared to other biomass sources, its potential has not been systematically investigated, particularly in the context of material development [8,9].

The growing demand for environmentally benign materials in agriculture has further highlighted the importance of utilizing biomass-derived polymers. In this context, agricultural and bio-based wastes are increasingly being reconsidered not merely as residues, but as valuable feedstocks for functional materials [3]. Notably, honeycomb waste contains various bioactive compounds such as flavonoids, tannins, and alkaloids, which are associated with antimicrobial and chemical stability properties. These characteristics indicate that the material may exhibit advantageous physicochemical behavior when processed into biopolymeric structures [4], [8].

Despite this potential, current *Trigona* beekeeping practices are primarily oriented toward harvesting high-value products, while the residual honeycomb material is often discarded or underutilized. This represents a missed opportunity for value addition, particularly in regions with active stingless bee cultivation [9], [10]. Converting such waste into functional biopolymers could contribute not only to waste minimization but also to the development of sustainable materials for agricultural applications. In particular, biopolymers with tailored structural and surface properties have attracted interest for various environmental, agricultural, and biomaterial applications[10,11].

Previous studies on biomass-derived polymers have largely focused on lignocellulosic sources such as agricultural residues, where cellulose extraction typically involves delignification processes through alkaline, enzymatic, or physicochemical treatments [12,13]. For instance, banana stem waste has been reported to yield cellulose with relatively high purity, although residual lignin and hemicellulose often remain, affecting material performance [14]. These findings underscore the importance of comprehensive physicochemical characterization in assessing the quality and applicability of biopolymers derived from alternative biomass sources [13-15].

Although various lignocellulosic wastes have been investigated as sources of cellulose-based biopolymers, the utilization of Trigona honeycomb waste remains largely unexplored. Most previous studies have focused on agricultural residues, wood-derived biomass, and plant fibers, whereas honeycomb waste generated from stingless bee cultivation has received limited scientific attention despite its abundance and renewable nature. Therefore, the present study introduces Trigona honeycomb waste as an alternative biomass resource for the production of cellulose-rich biopolymers and provides a comprehensive physicochemical characterization of the resulting material.

In this regard, the transformation of *Trigona* honeycomb waste into biopolymeric material requires systematic investigation, particularly in terms of structural modification and surface characteristics. Chemical activation processes are known to alter the morphology and functional groups of biomass-derived materials, potentially enhancing their performance in specific applications. However, such modifications have not been extensively studied for *Trigona*-based materials [8-10].

Therefore, this study aims to isolate cellulose-rich biopolymers from Trigona honeycomb waste and evaluate the influence of chemical activation on their physicochemical properties. Comprehensive characterization was conducted using XRF, XRD, FTIR, and SEM analyses to investigate changes in elemental composition, crystallinity, functional groups, and surface morphology. The resulting data are intended to establish a fundamental understanding of the material characteristics and provide a basis for future studies exploring specific functional applications of Trigona-derived biopolymers.

# Materials and Methods

## Materials and Chemicals

Trigona honeycomb waste was collected from local stingless bee (Trigona sp.) cultivation facilities in South Sulawesi, Indonesia. Distilled water was used throughout all experimental procedures. Sulfuric acid ($H_2SO_4$, 98%, analytical grade), sodium hydroxide (NaOH, ≥98%, analytical grade), sodium hypochlorite (NaClO, laboratory grade, 10–12% available chlorine), glacial acetic acid ($CH_3COOH$, ≥99.7%, analytical grade), and ethanol (96% (v/v), analytical grade) were purchased from Merck (Darmstadt, Germany). All chemicals were used as received without further purification.

## Raw Materials Preparation

Trigona honeycomb waste was collected from stingless bee cultivation facilities and manually cleaned to remove visible impurities. Approximately 50 g of honeycomb waste was collected from the honeycomb wall region, which is rich in lignocellulosic material. The raw material was initially washed with distilled water and cut into small pieces of approximately 1 cm. To remove residual waxes, honey residues, and other soluble organic compounds, the material was washed three times using 96% (v/v) ethanol under continuous stirring on a hot-plate stirrer for 1 h during each washing cycle [16]. The

cleaned material was subsequently air-dried for 3 h and then kept at room temperature for 24 h to ensure complete evaporation of residual ethanol [15]. The overall preparation procedure of Trigona honeycomb waste is illustrated in **Figure 1**.


**Figure 1.** Preparation Stage of Trigona Honeycomb Waste

## Isolation of Natural Biopolymers

Natural biopolymers were isolated from the prepared raw material through a sequential pulping process involving several chemical treatments. Initially, acid hydrolysis was carried out using 400 mL of 0.4% sulfuric acid ($H_2SO_4$) at 40°C for 1 h under constant stirring. This step was followed by a chlorination process using 400 mL of 3.5% sodium hypochlorite (NaClO) solution at the same temperature and duration. The treated sample was then washed repeatedly with distilled water until neutral pH was achieved. Subsequently, alkaline extraction was performed using 400 mL of 20% sodium hydroxide (NaOH) solution under continuous stirring for 1 h to remove non-cellulosic components. The sample was again washed to neutral pH and subjected to a bleaching step using 400 mL of 0.5% NaClO solution for 1 h. After completion of the chemical treatments, the sample was thoroughly washed until neutral, mechanically ground to obtain a more homogeneous structure, and then left at room temperature for 24 h. The material was further dried at 60°C and stored for an additional 24 h prior to activation [16]. The sequence of the isolation process is presented in **Figure 2**.

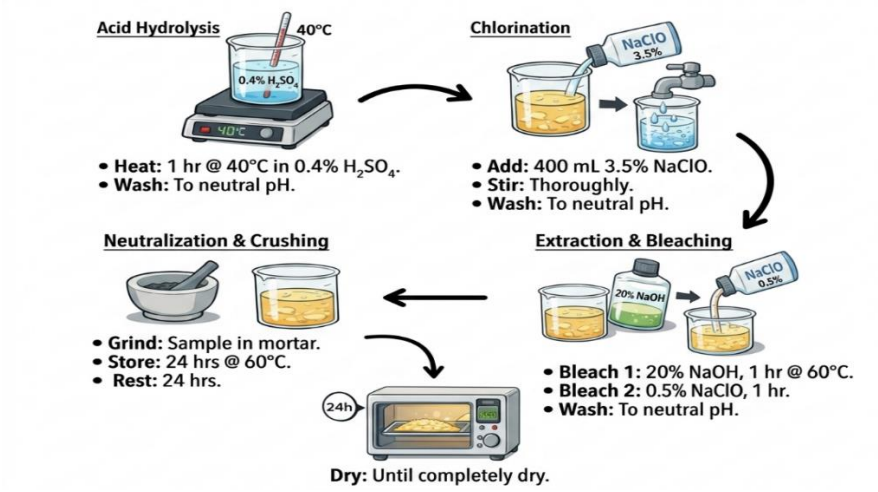


**Figure 2.** Isolation of Natural Biopolymers

## Activation Process of Natural Biopolymers

To investigate the effect of chemical activation, two types of samples were prepared, namely non-activated biopolymers and chemically activated biopolymers. For the activation process, 4 g of isolated biopolymer was immersed in a mixture consisting of 100 mL of glacial acetic acid ($CH_3COOH$) and 5 mL of sulfuric acid ($H_2SO_4$), corresponding to a solid-to-liquid ratio of approximately 1:26 (w/v) [15], [16]. The suspension was continuously stirred and heated at 40°C for 3 h.

The activation conditions were selected based on previously reported procedures for cellulose-rich biomass modification [15], [16]. Acetic acid serves as a mild organic acid capable of facilitating surface

modification and removing residual impurities, whereas sulfuric acid functions as a stronger acidic catalyst that promotes partial hydrolysis and structural rearrangement within the biopolymer matrix. The relatively low activation temperature (40°C) and moderate treatment duration (3 h) were employed to allow sufficient interaction between the activating agents and the cellulose-rich structure while minimizing excessive degradation of the polymer backbone.

After activation, the mixture was filtered to separate the solid fraction from the liquid phase. The recovered material was then dried in an oven at 60°C until constant weight was achieved and subsequently stored in sealed containers prior to characterization. The activation procedure is depicted in Figure 3.

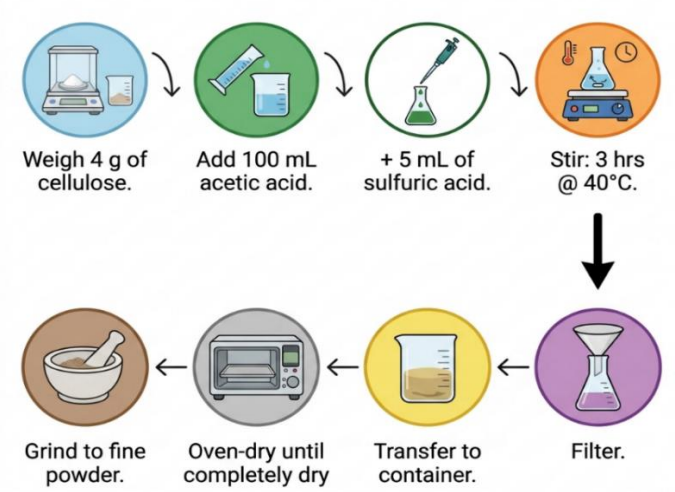


**Figure 3.** Activation process of natural biopolymers derived from Trigona honeycomb waste.

## Characterization Techniques

The physicochemical characterization of the prepared biopolymers was conducted at the Integrated Central Laboratory (Sentral Laboratory), Universitas Negeri Malang, Indonesia.

Elemental composition was analyzed using an X-ray fluorescence spectrometer (PANalytical Minipal 4) operated at 30 kV. The elemental concentrations were determined and reported as relative weight percentages.

Crystalline structure analysis was performed using an X-ray diffractometer (PANalytical X'Pert PRO) employing Cu-Kα radiation (λ = 1.5406 Å), operated at 40 kV and 30 mA. Diffraction data were collected over a 2θ range of 5–80° with a scanning rate of 2° $min^{-1}$. Phase identification was carried out by comparing the diffraction peaks with reference patterns reported in the literature.

Functional groups were identified using a Fourier transform infrared spectrometer (Shimadzu IRPrestige-21, Shimadzu Corporation, Japan). Spectra were recorded in the wavenumber range of 4000–400 $cm^{-1}$ with a spectral resolution of 4 $cm^{-1}$ and 32 accumulated scans for each measurement.

Surface morphology was examined using a scanning electron microscope (FEI Inspect-S50, FEI Company, USA) operated at an accelerating voltage of 15 kV. Micrographs were obtained at magnifications of 250×, 1000×, and 2000×. Prior to SEM observation, the samples were sputter-coated with a thin layer of gold to improve conductivity and minimize charging effects during imaging.

# Results and Discussion

## Elemental Composition Analysis

The elemental composition of the biopolymer derived from *Trigona* honeycomb waste was evaluated using X-ray fluorescence (XRF) [17] before and after chemical activation. As summarized in **Table 1**, calcium (Ca) was identified as the predominant element in both samples, with its relative content increasing from 46.6% to 54.8% after activation. A similar increasing trend was observed for other elements, including potassium (K), iron (Fe), manganese (Mn), nickel (Ni), and copper (Cu).

This compositional shift can be associated with the progressive removal of organic constituents during the pulping and activation stages [18]. Treatments involving acid hydrolysis, alkaline extraction, and bleaching are known to reduce lignin, hemicellulose, and other amorphous organic fractions, thereby enriching the relative proportion of inorganic mineral components [19,20]. As a result, elements initially embedded within the organic matrix become more exposed or concentrated in the residual structure.

Notably, the increase in potassium content from 12.0% to 15.6% suggests enhanced availability of alkali

metals after activation, which may influence the material's surface reactivity and ionic interaction capacity [21,22]. Likewise, the enrichment of calcium indicates that mineral phases associated with the honeycomb matrix remain stable under the applied treatment conditions [23,24]. This behavior implies that the activation process primarily alters the organic framework while preserving or concentrating mineral constituents.

**Table 1**. Elemental composition of natural biopolymers before and after activation

| 42 | Before Activation (%) | After Activation (%) |
|---|---|---|
| P | 4,6 | 4,7 |
| S | 9,3 | 9,3 |
| K | 12 | 15,6 |
| Ca | 46,6 | 54,8 |
| Mn | 2,3 | 3,0 |
| Fe | 4,9 | 6,6 |
| Ni | 1,5 | 2,1 |
| Cu | 2,4 | 3,9 |

The oxide composition further supports these observations, as presented in **Table 2**. Calcium oxide (CaO) remained the dominant phase, increasing from 44.1% to 49.2% after activation. Potassium oxide ($K_2O$) also exhibited a noticeable rise, from 9.6% to 12.9%, whereas phosphorus oxide ($P_2O_5$) showed only a marginal increase. In contrast, sulfur oxide ($SO_3$) remained relatively constant at approximately 17%, indicating that sulfur-containing compounds are less affected by the activation conditions. Because XRF provides elemental composition in relative percentage terms, the observed increase in calcium concentration should be interpreted cautiously. The activation process may preferentially remove organic fractions such as residual lignocellulosic components, thereby increasing the proportional contribution of mineral species within the analyzed sample. Consequently, the results indicate relative calcium enrichment rather than direct calcium accumulation [23], [26].

The enrichment of oxide species can be interpreted as a concentration effect resulting from the removal of volatile and degradable organic fractions [25]. In addition, the persistence of CaO and $K_2O$ suggests that these mineral phases are structurally stable and may contribute to the overall rigidity and chemical functionality of the material [26]. Minor increases in transition metal oxides such as $Fe_2O_3$, MnO, NiO, and CuO further indicate that trace elements are retained within the matrix, potentially influencing surface properties and interaction behavior [23], [26].

Table 2. Oxide composition of natural biopolymers before and after activation.

| Oxide | Before Activation (%) | After Activation (%) |
|---|---|---|
| $P_2O_5$ | 8.1 | 8.3 |
| $SO_3$ | 17.0 | 17.0 |
| $K_2O$ | 9.6 | 12.9 |
| CaO | 44.1 | 49.2 |
| MnO | 1.9 | 2.3 |
| $Fe_2O_3$ | 4.6 | 5.6 |
| NiO | 1.2 | 1.5 |
| CuO | 1.9 | 2.9 |

Overall, the XRF results indicate that chemical activation does not introduce new elemental species but rather modifies the relative composition by reducing organic matter and concentrating mineral components [27,28]. This compositional evolution is particularly relevant in the context of biomass-derived materials, where mineral-rich structures may influence physicochemical behavior such as surface charge, ion exchange capacity, and interaction with surrounding media. Consequently, the observed enrichment of Ca- and K-based compounds suggests that the activated biopolymer may serve as a mineral-containing matrix with potential functional applications, although further performance evaluation is required to substantiate this role [27,28].

## Crystallinity Analysis

The crystalline structure of the cellulose-rich biopolymer derived from Trigona honeycomb waste was investigated using X-ray diffraction (XRD), and the resulting diffractogram is presented in Figure 4. The diffraction pattern exhibits characteristic reflections at 2θ values of approximately 11.65°, 14.81°, 15.99°,

20.81°, and 23.23°, which are commonly associated with cellulose type I [29,30]. These diffraction peaks correspond to the crystallographic planes (1$\bar{1}$0), (101), (110), and (200), indicating that the fundamental cellulose crystalline framework was preserved throughout the isolation and activation processes [31,32].

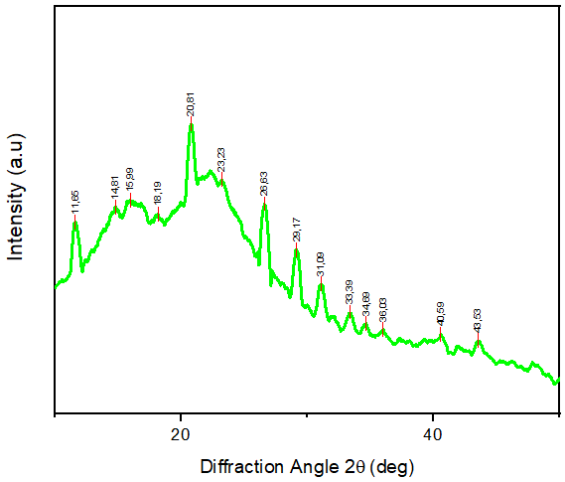


**Figure 4.** XRD pattern of activated natural biopolymers derived from *Trigona* honeycomb waste.

Among the observed reflections, the diffraction peak located within the range of 20.81°–23.23° is attributed to the (200) plane, which represents the principal crystalline region of cellulose. The presence of this peak confirms the retention of ordered cellulose domains following chemical treatment. In addition, a broad diffraction feature observed around 18° indicates the presence of amorphous regions within the material. The coexistence of crystalline and amorphous domains suggests that the isolated material exhibits a semi-crystalline structure, which is characteristic of many cellulose-based materials derived from lignocellulosic biomass [30,31].

Besides the cellulose-related reflections, several minor diffraction peaks were detected at higher diffraction angles. Peaks located at approximately 26.63° and 29.17° may be attributed to quartz ($SiO_2$) and calcite ($CaCO_3$), respectively, while additional low-intensity reflections above 30° are likely associated with calcium-containing mineral phases and silicate-related compounds [33,34]. The presence of these inorganic phases is consistent with the XRF results, which revealed the occurrence of mineral constituents originating from the original honeycomb matrix.

Slight peak broadening was observed in several diffraction regions, suggesting that chemical activation may have induced structural rearrangements within the cellulose-rich matrix. Acidic and alkaline treatments are known to modify intermolecular hydrogen-bonding networks and partially remove amorphous constituents, which can influence the structural organization of cellulose-based materials [35], [36]. However, because crystallinity index calculations and crystallite size analyses were not performed in the present study, the extent of these structural modifications cannot be quantitatively determined from the available diffraction data.

Overall, the XRD analysis demonstrates that the isolated material retains the characteristic diffraction features of cellulose type I while exhibiting a semi-crystalline structure containing both ordered and amorphous domains (Table 3). The detection of minor mineral-associated reflections further indicates that a fraction of the inorganic constituents originating from the honeycomb biomass remained after chemical processing. Although the diffraction patterns provide evidence of structural preservation following activation, quantitative analyses such as crystallinity index determination would be required to establish a more detailed relationship between structural organization and material performance.

**Table 3.** XRD analysis results of activated natural biopolymers [37,38]

| 2Θ(°) | Identified Phase | Field (hkl) | Information |
|---|---|---|---|
| 11,65 | Cellulose type I | (1$\bar{1}$0) | Weak crystalline reflection |
| 14,81 | Cellulose type I | (101) | Characteristics of crystalline cellulose |

| | | | |
|---|---|---|---|
| 15,99 | Cellulose type I | (110) | Semi-crystalline structure |
| 18,19 | Cellulose (amorf) | – | Amorphous region |
| 20,81 | Cellulose type I | (200) | Main crystalline peak |
| 23,23 | Cellulose type I | (200) | Dominant crystalline reflection |
| 26,63 | $SiO_2$ (quartz) | (101) | Mineral minor |
| 29,17 | $CaCO_3$ (calcite) | (104) | Carbonate residue |
| 31,09 | CaO/ minor silicates | (111) | Minor inorganic phase |
| 33,39 | CaO/mineral minor | – | Low intensity |
| 34,39 | Inorganic minerals | – | Impurity |
| 36,03 | CaO | (200) | Minor phase |
| 40,59 | Cao/silicates | – | Minor |
| 43,53 | CaO | (220) | Minor |

## Functional Group Analysis

Fourier transform infrared (FTIR) spectroscopy was employed to identify the functional groups present in the biopolymer derived from *Trigona* honeycomb waste [39]. The spectrum, shown in **Figure 5**, exhibits several characteristic absorption bands associated with cellulose-based materials.

A broad absorption band centered around 3420 $cm^{-1}$ is attributed to O–H stretching vibrations, indicating the presence of extensive hydrogen bonding within the polymeric network [40,41]. This feature is typical for polysaccharide structures and reflects intermolecular and intramolecular interactions between hydroxyl groups. The absorption band observed at approximately 2930 $cm^{-1}$ corresponds to aliphatic C–H stretching vibrations, which are commonly associated with the cellulose backbone [42,43].

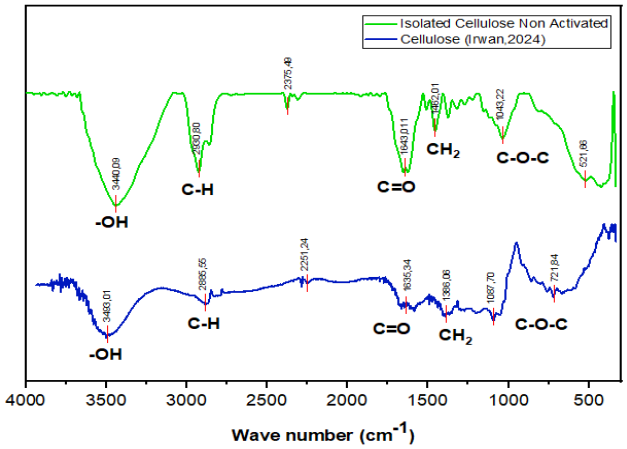


**Figure 5.** FTIR spectrum of natural biopolymers derived from *Trigona* honeycomb waste.

The absorption band observed at approximately 1643 $cm^{-1}$ is commonly associated with the bending vibration of absorbed water molecules (H–O–H) retained within the cellulose structure through hydrogen-bonding interactions [41], [42]. This band is frequently reported in cellulose-based materials due to their hydrophilic nature and ability to retain moisture within amorphous and accessible regions of the polymer network. In addition, a minor contribution from carbonyl-containing groups generated during chemical treatment cannot be completely excluded. Therefore, the band at 1643 $cm^{-1}$ is more appropriately interpreted as arising predominantly from absorbed water, with possible overlap from limited oxidative functionalities[41], [43]. The moderate intensity of this absorption suggests that the chemical treatment did not induce extensive oxidation of the cellulose-rich matrix. In addition, the presence of a peak around 1462 $cm^{-1}$ is attributed to $CH_2$ bending vibrations, further supporting the structural integrity of the cellulose chains.

A prominent absorption band at approximately 1043 $cm^{-1}$ corresponds to C–O–C stretching vibrations, which are characteristic of β-1,4-glycosidic linkages in cellulose. This peak serves as a key indicator of the polysaccharide framework and confirms that the fundamental backbone structure remains intact after the isolation and activation processes [41], [44].

Importantly, the absence or significant reduction of absorption bands in the region of 1500–1700 $cm^{-1}$, typically associated with lignin aromatic structures, indicates that non-cellulosic components have been effectively removed during the pulping and bleaching stages. This observation is consistent with the XRD

results, which suggest a relatively purified cellulose structure with reduced amorphous impurities.
To further validate the structural assignment, the FTIR spectrum of the extracted biopolymer was compared with reference cellulose derived from sengon wood, as summarized in **Table 4**. The comparison shows a high degree of similarity in the major absorption bands, particularly in the regions corresponding to O–H (~3420 $cm^{-1}$), C–H (~2930 $cm^{-1}$), C=O (~1643 $cm^{-1}$), $CH_2$ (~1462 $cm^{-1}$), and C–O–C (~1043 $cm^{-1}$) [44]. These similarities indicate that the chemical structure of the isolated material closely resembles that of conventional cellulose.

**Table 4**. Table 4. Comparison of characteristic FTIR absorption bands of the isolated biopolymer with cellulose reported in the literature

| Trigona honeycomb waste cellulose (Data Primer, 2026) | | Sengon wood cellulose [44] | |
|---|---|---|---|
| Wave number ($cm^{-1}$) | Funtional group | Wave number ($cm^{-1}$) | Funtional group |
| 3420 | -OH | 3333 | -OH |
| 2930 | C-H | 2289/~2900 | C-H |
| 1643 | Adsorbed water (H–O–H bending), possible C=O overlap | 1647 | C=O |
| 1462 | $CH_2$ | ~1430/1450 | $CH_2$ |
| 1043 | C-O-C | 1028 | C-O-C |
| ~2375 | $CO_2$ atmosfer | - | - |

To further support the identification of the isolated material as a cellulose-rich biopolymer, the obtained FTIR spectrum was compared with reference cellulose spectra reported in the literature, including cellulose derived from Sengon wood [44]. This comparison was performed because cellulose extracted from different biomass sources generally exhibits similar characteristic absorption bands associated with hydroxyl, aliphatic, and glycosidic functional groups. The major absorption bands observed in the present study at approximately 3420 $cm^{-1}$ (O–H stretching), 2930 $cm^{-1}$ (C–H stretching), 1643 $cm^{-1}$ (C=O stretching), 1462 $cm^{-1}$ ($CH_2$ bending), and 1043 $cm^{-1}$ (C–O–C stretching) closely correspond to those reported for cellulose in previous studies. The agreement between these characteristic bands indicates that the isolated material possesses the fundamental chemical features of cellulose.
Rather than demonstrating equivalence between Trigona honeycomb cellulose and Sengon wood cellulose, the comparison serves as supporting evidence for functional group assignment. The observed spectral similarity confirms the preservation of the cellulose backbone following the isolation and activation processes, while the reduced intensity of bands commonly associated with lignin and other non-cellulosic constituents suggests substantial purification of the biopolymer fraction.
Overall, the FTIR analysis confirms that the extracted material retains the functional groups characteristic of cellulose, with minimal interference from lignin and hemicellulose components. The preservation of hydroxyl-rich functional groups, combined with the stability of glycosidic linkages, suggests that the chemical treatment primarily removes impurities while maintaining the polymer framework. This structural integrity is essential for applications requiring stable yet reactive biopolymeric matrices, particularly those involving surface interactions and molecular diffusion processes.

## Morphological Analysis

The surface morphology of the activated biopolymer derived from Trigona honeycomb waste was examined using scanning electron microscopy (SEM) at different magnifications, as presented in Figures 6a–6c. Figure 6a (250× magnification) provides an overview of the surface morphology at the microscale. The image reveals an irregular and heterogeneous surface characterized by uneven topography and localized discontinuities. The absence of a smooth and compact surface indicates that the chemical treatment modified the original biomass structure, resulting in a more accessible surface morphology.At a higher magnification of 1000× (Figure 6b), surface roughness becomes more pronounced, and several pores and microcavities can be clearly observed. These features are likely associated with the removal of non-cellulosic constituents and amorphous phases during the acid, alkaline, and bleaching treatments. The formation of these voids suggests that the isolation and activation processes promoted the development of a more open structure. Figure 6c (2000× magnification) reveals finer microstructural details of the activated biopolymer. Numerous interconnected pores, small cavities, and localized fractures are visible throughout the surface. The appearance of these features indicates substantial

structural reorganization at the microscale, which may be attributed to the disruption of intermolecular interactions and partial removal of residual impurities during chemical processing [45,46].
The progressive increase in visible surface features from Figures 6a to 6c demonstrates the heterogeneous and porous nature of the activated biopolymer. Such morphological characteristics are consistent with the XRD results indicating structural modification and with the FTIR analysis showing the removal of non-cellulosic components while preserving the cellulose backbone. The formation of pores and microcavities may enhance the accessibility of active sites and facilitate interactions with surrounding media, which is advantageous for applications requiring efficient mass transfer and surface-mediated processes [47,48].

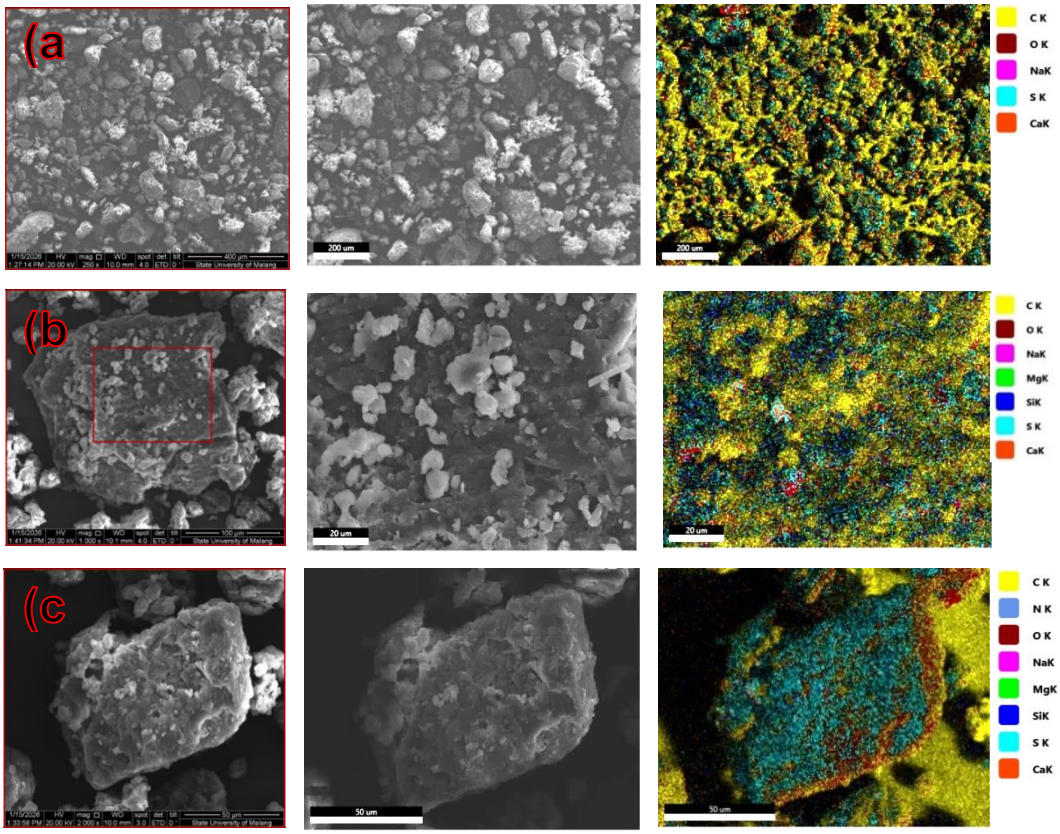


**Figure 6.** Figure 6. SEM micrographs of activated biopolymers derived from Trigona honeycomb waste at different magnifications: (a) 250×, (b) 1000×, and (c) 2000×

To further quantify the morphological features, particle size distribution analysis was conducted using Gaussian fitting [49,50], as shown in **Figure 7**. The analysis indicates an average particle size of approximately 263.55 nm with a relatively normal distribution profile. The presence of a near-symmetric distribution suggests a reasonably uniform particle population, although slight deviations indicate minor agglomeration.

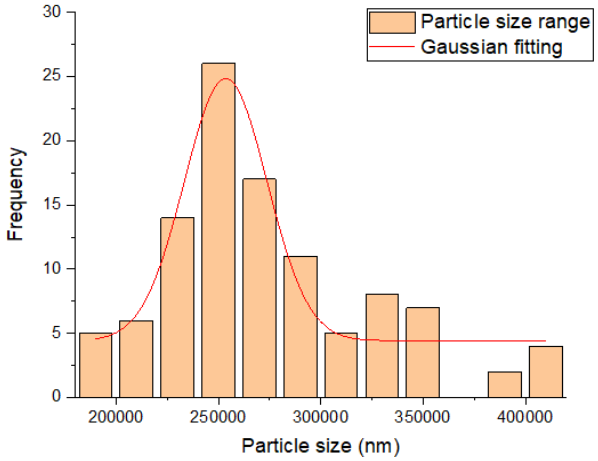


**Figure 7.** Particle size distribution of natural biopolymers obtained through Gaussian fitting analysis.

The observed agglomeration may be attributed to intermolecular interactions between hydroxyl groups, which can promote particle clustering during drying or sample preparation [51]. Despite this, the overall distribution remains sufficiently narrow, indicating that the processing conditions yield a relatively homogeneous material. Such characteristics are relevant for applications requiring consistent surface properties, particularly in systems involving coating or interfacial contact [49,50]. The SEM observations reveal that the activated cellulose-rich biopolymer possesses a heterogeneous surface characterized by rough textures, interconnected pores, microcavities, and localized fractures. These morphological features are consistent with the structural characteristics identified by XRD and FTIR analyses and suggest that the chemical treatment produced a porous cellulose-based material with increased surface accessibility. Such surface characteristics may be beneficial for applications involving adsorption, interfacial interactions, and mass-transfer processes.

## Conclusion

This study demonstrates that natural biopolymers can be effectively isolated from *Trigona* honeycomb waste through a sequential pulping process involving acid hydrolysis, chlorination, alkaline extraction, and bleaching. The combined characterization results consistently indicate that the extracted material is predominantly cellulose-based with a semi-crystalline structure (cellulose type I). XRD analysis confirms the preservation of the crystalline framework, while FTIR spectra verify the presence of functional groups, including hydroxyl (–OH), aliphatic C–H, and glycosidic C–O–C linkages. Elemental analysis by XRF reveals that calcium (Ca) is the dominant component, with an increased relative concentration after activation, accompanied by other mineral elements such as K, P, and S. These changes are associated with the removal of organic constituents during processing, leading to mineral enrichment within the material. Morphological observations from SEM further show a clear transformation from a compact structure to a more heterogeneous and porous surface after activation, indicating the formation of microcavities and increased surface irregularity. Taken together, these findings demonstrate that chemical treatment not only preserves the structural features of cellulose but also modifies the physicochemical properties of the material, particularly in terms of mineral composition and surface morphology. Such characteristics suggest that the obtained biopolymer may serve as a promising biomass-derived precursor for functional material development. However, further studies focusing on performance evaluation, such as controlled release behavior and interaction with environmental media, are required to substantiate its application in sustainable agricultural systems.

## Conflicts of Interest

The author(s) declare(s) that there is no conflict of interest regarding the publication of this paper.

## Acknowledgment

The authors gratefully acknowledge financial support from the Lembaga Pengelola Dana Pendidikan (LPDP) and the National Research and Innovation Agency (BRIN) through the Riset untuk Indonesia Maju (RIIM) scheme under contract numbers 109/IV/KS/07/2025 and 133/LPPM/UNCP/VII/2025.

## References

[1] L. Abdulsalam *et al.*, "Advanced biocompatible and biodegradable polymers: A review of functionalization, smart systems, and sustainable applications," *Polymers (Basel).*, vol. 17, no. 21, p. 2901, 2025.

[2] M. Z. Al Mahmud, M. D. Islam, and M. H. Mobarak, "The Development of Eco- Friendly Biopolymers for Use in Tissue Engineering and Drug Delivery," *J. Nanomater.*, vol. 2023, no. 1, p. 9270064, 2023.

[3] T. Fazal *et al.*, "Recent developments in natural biopolymer based drug delivery systems," *RSC Adv.*, vol. 13, no. 33, pp. 23087–23121, 2023.

[4] S. Gulati *et al.*, "Nanobiopolymers in cancer therapeutics: advancing targeted drug delivery through sustainable and controlled release mechanisms," *J. Mater. Chem. B*, vol. 12, no. 46, pp. 11887–11915, 2024.

[5] A. C. Q. Silva, A. J. D. Silvestre, C. Vilela, and C. S. R. Freire, "Natural polymers-based materials: A contribution to a greener future," *Molecules*, vol. 27, no. 1, p. 94, 2021.

[6] R. K. Pavithran, S. G. Reddy, B. S. Kumar, and S. Kugabalasooriar, "Enhancing sustainability in agriculture: natural polymer-based controlled release systems for effective pest management and environmental protection," *ES Food Agrofor.*, vol. 18, p. 1276, 2024.

[7] B. Zhang, B. K. Biswal, J. Zhang, and R. Balasubramanian, "Hydrothermal treatment of biomass feedstocks for sustainable production of chemicals, fuels, and materials: progress and perspectives," *Chem. Rev.*, vol. 123, no. 11, pp. 7193–7294, 2023.

[8] H. Alcocer-García, E. Sánchez-Ramírez, E. García-García, C. Ramírez-Márquez, and J. M. Ponce-Ortega, "Unlocking the potential of biomass resources: a review on sustainable process design and intensification," *Resources*, vol. 14, no. 9, p. 143, 2025.

[9] F. G. B. Bueno *et al.*, "Stingless bee floral visitation in the global tropics and subtropics," *Glob. Ecol. Conserv.*, vol. 43, p. e02454, 2023.

[10] S. Ghosh, D. P. Abrol, and C. Jung, "The State of Beekeeping in India: Insights, Gaps, and Emerging Opportunities," *Entomol. Res.*, vol. 55, no. 10, p. e70069, 2025.

[11] O. Duangphakdee, J. Baroga-Barbecho, P. Rod-Im, K. Attasopa, A. Locsin, and C. Cervancia, "Economic Feasibility and Income Security of Stingless Bee Keeping for Small-Holder Farmers in Southeast Asia," in *Stingless Bee Nest Cerumen and Propolis, Volume 1*, Springer, 2024, pp. 3–31.

[12] T. Mkilima, "Harnessing alkaline-treated agricultural residues for dual-function bioadsorbents and biopolymer precursors," *Biotechnol. Sustain. Mater.*, vol. 2, no. 1, p. 26, 2025.

[13] A. A. Dandash, B. Abu- Jdayil, and J. H. Tannous, "Lignin extraction from various biomass sources: A comprehensive review of Characteristics, Applications, and future prospects," *Chem. Rec.*, vol. 25, no. 8, p. e202500045, 2025.

[14] A. Waithaka *et al.*, "Cellulose-Based biopolymers from banana pseudostem waste: innovations for sustainable bioplastics," in *Waste*, MDPI, 2025, p. 37.

[15] S. I. Abro *et al.*, "Valorization strategy for biodegradable products of tissues and paper sheets made from banana pseudostem pulp," *Biomass and Bioenergy*, vol. 207, p. 108707, 2026.

[16] M. Sengar *et al.*, "Extraction of plant wax from Colocasia esculenta using polar and non-polar solvents: A sustainable approach," *Biomass Convers. Biorefinery*, vol. 15, no. 22, pp. 29401–29413, 2025.

[17] H. O. Onovo, A. A. Agbeleye, T. T. Akano, D. B. Oludele, J. O. Olawoyin, and I. S. Kentosu, "Comprehensive Study of Extraction and Applicability of Nanosilicate Particles from Natural Waste for Biopolymer Reinforcement," *Niger. J. Technol.*, vol. 43, no. 4, pp. 666–675, 2024.

[18] S. Balkissoon, J. Andrew, and B. Sithole, "Dissolving wood pulp production: a review," *Biomass Convers. biorefinery*, vol. 13, no. 18, pp. 16607–16642, 2023.

[19] Z. Huang *et al.*, "Unravelling sequence-dependent molecular transformation pathways of dissolved organic matter in chemical cleaning wastewater during combined Fenton oxidation and activated carbon adsorption processes," *Sep. Purif. Technol.*, p. 134335, 2025.

[20] D. Mboowa, "A review of the traditional pulping methods and the recent improvements in the pulping processes," *Biomass Convers. Biorefinery*, vol. 14, no. 1, pp. 1–12, 2024.
[21] J. Jiang, H. Wang, J. Ren, L. Deng, and D. Che, "Effect of inherent alkali and alkaline earth metals in biochar on adsorption of Pb2+ in aqueous solution: different roles of Na/Mg/K/Ca," *Sep. Purif. Technol.*, vol. 354, p. 128766, 2025.
[22] R. Murugavel, A. A. Rownaghi, and F. Rezaei, "Effect of alkali metal functionalization on hydrogen storage performance of highly porous activated carbons," *Energy & fuels*, vol. 37, no. 23, pp. 19292–19303, 2023.
[23] Z. Deng, Z. Jia, and L. Li, "Biomineralized materials as model systems for structural composites: Intracrystalline structural features and their strengthening and toughening mechanisms," *Adv. Sci.*, vol. 9, no. 14, p. 2103524, 2022.
[24] L. Zhou *et al.*, "Honeycomb-like macroporous crosslinked chitosan assisted EDTA-intercalated Ca-Mg-Al layered hydrotalcite composite foams for efficient U (VI) biosorption," *Int. J. Biol. Macromol.*, vol. 279, p. 135011, 2024.
[25] Y. Zhang *et al.*, "Photocatalytic oxidation for volatile organic compounds elimination: from fundamental research to practical applications," *Environ. Sci. Technol.*, vol. 56, no. 23, pp. 16582–16601, 2022.
[26] P. Tuo, Z. Zhang, P. Du, L. Hu, R. Li, and J. Ren, "Changes in coal waste DOM chemodiversity and Fe/Al oxides during weathering drive the fraction conversion of heavy metals," *Sci. Total Environ.*, vol. 926, p. 172063, 2024.
[27] A. Cinosi, G. Siviero, and Z. McCaffrey, "Elemental analysis of valuable byproducts by TXRF spectrometry: coal fly ash and activated carbon," *Spectrochim. Acta Part B At. Spectrosc.*, vol. 220, p. 107017, 2024.
[28] T. R. Tavares, E. de Almeida, C. R. P. Junior, A. Guerrero, P. R. Fiorio, and H. W. P. de Carvalho, "Analysis of total soil nutrient content with X-ray Fluorescence Spectroscopy (XRF): Assessing different predictive modeling strategies and auxiliary variables," *AgriEngineering*, vol. 5, no. 2, pp. 680–697, 2023.
[29] N. S. Syazwani, M. N. E. Efzan, C. K. Kok, and M. J. Nurhidayatullaili, "Analysis on extracted jute cellulose nanofibers by Fourier transform infrared and X-Ray diffraction," *J. Build. Eng.*, vol. 48, p. 103744, 2022.
[30] M.-C. Stanciu, F. Tanasă, and C.-A. Teacă, "Crystallinity changes in modified cellulose substrates evidenced by spectral and X-ray diffraction data," *Polysaccharides*, vol. 6, no. 2, p. 30, 2025.
[31] F. CHERIFI, "Extraction, physico-chemicaland morphological analysis of bioproducts from date palm by-products in southern Algeria, and applications.," *université Kasdi Merbah ouargla*.
[32] H. Tesfaye, T. Gabriel, N. M. Joseph, and T. Gebre-Mariam, "Comparative Analysis of Cellulose Characteristics from Three Agricultural Waste Biomasses," *J. Nat. Fibers*, vol. 22, no. 1, p. 2578610, 2025.
[33] Y. Huang, G. Huang, Z. Han, F. Zhang, M. Liu, and J. Hao, "Evolution of Mechanical Properties, Mineral Crystallization, and Micro-Gel Formation in Alkali-Activated Carbide Slag Cementitious Materials," *Crystals*, vol. 15, no. 8, p. 731, 2025.
[34] N. Böhme, K. Hauke, M. Dohrn, M. Neuroth, and T. Geisler, "High-temperature phase transformations of hydroxylapatite and the formation of silicocarnotite in the hydroxylapatite–quartz–lime system studied in situ and in operando by Raman spectroscopy," *J. Mater. Sci.*, vol. 57, no. 32, pp. 15239–15266, 2022.
[35] J. Li and M. Hitch, "Characterization of the microstructure of mechanically-activated olivine using X-ray diffraction pattern analysis," *Miner. Eng.*, vol. 86, pp. 24–33, 2016.
[36] P. Pourghahramani and E. Forssberg, "Microstructure characterization of mechanically activated hematite using XRD line broadening," *Int. J. Miner. Process.*, vol. 79, no. 2, pp. 106–119, 2006.
[37] M. H. Mulla *et al.*, "Low velocity impact performance of natural fibre reinforced polymer composites: a review," *Funct. Compos. Struct.*, vol. 5, no. 3, p. 35004, 2023.
[38] M. H. Mulla, M. N. Norizan, N. F. M. Rawi, M. H. M. Kassim, N. Abdullah, and M. N. F. Norrrahim, "Surface and interfaces effects of concentrations and alkaline treatment durations on sugar palm fiber as structural reinforcement in polymer composites," *J. Nat. Fibers*, vol. 22, no. 1, p. 2527277, 2025.
[39] S. V. María *et al.*, "Biopolymer production by bacteria isolated from native stingless bee honey, Scaptotrigona jujuyensis," *Food Biosci.*, vol. 42, p. 101077, 2021.
[40] S. Azeez and R. Shenbagaraman, "Fourier transform infrared spectroscopy in characterization of bionanocomposites," in *Characterization Techniques in Bionanocomposites*, Elsevier, 2025, pp. 209–227.
[41] M. O. Yusuf, "Bond characterization in cementitious material binders using Fourier-transform infrared spectroscopy," *Appl. Sci.*, vol. 13, no. 5, p. 3353, 2023.
[42] R. Md Salim, J. Asik, and M. S. Sarjadi, "Chemical functional groups of extractives, cellulose

and lignin extracted from native Leucaena leucocephala bark," *Wood Sci. Technol.*, vol. 55, no. 2, pp. 295–313, 2021.
[43] H. G. Higgins, C. M. Stewart, and K. J. Harrington, "Infrared spectra of cellulose and related polysaccharides," *J. Polym. Sci.*, vol. 51, no. 155, pp. 59–84, 1961.
[44] N. Ikhtiarini, M. Masruri, and S. M. Ulfa, "Synthesis and Characterization of Cellulose Acetate and Nanocellulose Acetate from Sengon Agroindustrial Waste (Paraserianthes falcataria).," *J. Pure Appl. Chem. Res.*, vol. 11, no. 3, 2022.
[45] O. El Samrout, "Molecules at surfaces: formation, reactivity, assembly of (bio) molecules on external and internal surfaces of nanosized/nanostructured materials," 2023.
[46] Z. Tang, "Fabrication of Surfaces With Controlled Wetting Properties on Porous Substrates Using Nonfluorinated Chemicals," 2016, *Georgia Institute of Technology*.
[47] S. Li, G. Ni, H. Wang, M. Xun, and Y. Xu, "Effects of acid solution of different components on the pore structure and mechanical properties of coal," *Adv. Powder Technol.*, vol. 31, no. 4, pp. 1736–1747, 2020.
[48] J. Kang, X. Yang, Q. Hu, Z. Cai, L.-M. Liu, and L. Guo, "Recent progress of amorphous nanomaterials," *Chem. Rev.*, vol. 123, no. 13, pp. 8859–8941, 2023.
[49] A. Mazzoli and O. Favoni, "Particle size, size distribution and morphological evaluation of airborne dust particles of diverse woods by Scanning Electron Microscopy and image processing program," *Powder Technol.*, vol. 225, pp. 65–71, 2012.
[50] S. F. Islam, S. M. Hawkins, J. L. L. Meyer, and A. R. C. Sharman, "Evaluation of different particle size distribution and morphology characterization techniques," *Addit. Manuf. Lett.*, vol. 3, p. 100077, 2022.
[51] S. P. Yeap, "Permanent agglomerates in powdered nanoparticles: Formation and future prospects," *Powder Technol.*, vol. 323, pp. 51–59, 2018.